Interlacing in Atomic Resolution Scanning Transmission Electron Microscopy

Jonathan J P Peters, Tiarnan Mullarkey, James A Gott, Elizabeth Nelson, Lewys Jones

Microscopy and Microanalysis, 2023, **29**, 1373–1379
https://doi.org/10.1093/micmic/ozad056
Advance access publication 7 June 2023
Original Article

Microscopy AND Microanalysis

Interlacing in Atomic Resolution Scanning Transmission Electron Microscopy

Jonathan J. P. Peters[1,2,*], Tiarnan Mullarkey[1,2,3], James A. Gott[4,5], Elizabeth Nelson[2], and Lewys Jones[1,2,3]

[1]*Advanced Microscopy Laboratory, Centre for Research on Adaptive Nanostructures and Nanodevices (CRANN), Trinity College Dublin, Dublin D02 DA31, Ireland*
[2]*School of Physics, Trinity College Dublin, Dublin D02 E8C0, Ireland*
[3]*Centre for Doctoral Training in the Advanced Characterisation of Materials, AMBER Centre, Trinity College Dublin, Dublin D02 W9K7, Ireland*
[4]*Department of Physics, University of Warwick, Coventry CV4 7AL, UK*
[5]*Advanced Materials Manufacturing Centre (AMMC), Warwick Manufacturing Group (WMG), University of Warwick, Coventry CV4 7AL, UK*

***Corresponding author:** Jonathan J. P. Peters, E-mail: jonathan.peters@tcd.ie

Abstract

Fast frame rates are desirable in scanning transmission electron microscopy for a number of reasons: controlling electron beam dose, capturing *in situ* events, or reducing the appearance of scan distortions. While several strategies exist for increasing frame rates, many impact image quality or require investment in advanced scan hardware. Here, we present an interlaced imaging approach to achieve minimal loss of image quality with faster frame rates that can be implemented on many existing scan controllers. We further demonstrate that our interlacing approach provides the best possible strain precision for a given electron dose compared with other contemporary approaches.

Key words: high frame-rate STEM, interlacing, scanning transmission electron microscopy, strain precision

Introduction

Scanning transmission electron microscopy (STEM) has become a widespread and powerful technique in materials science, particularly with the development of practical aberration correctors. An electron beam is focused on a spot, with a diameter as small as <100 pm (Sasaki et al., 2012) and is scanned across the surface of a material. As the beam is scanned, or rastered, across the material, multiple signals can be collected simultaneously using different detectors. For example, images can be formed based on scattering to annular dark field (ADF) or spectroscopic information can be retrieved from electron energy loss spectroscopy or energy dispersive X-ray spectrometers (Muller, 2009). Increasingly, segmented or pixelated detectors are being used to obtain more elaborate contrast mechanisms (Ophus, 2019).

The ability to gather these multiple signals at atomic resolution is one of the main merits of STEM. However, the serial fashion of the scanning process is relatively slow compared with parallel high-resolution transmission electron microscopy (HRTEM). In conventional scanning, this drawback is compounded by an additional flyback wait time at the beginning of each scan line, used to allow for lens hysteresis effects to decay. There is then another similar wait time between each frame, though this may also compensate for limited data streaming bandwidth or other delays. The total time for an image to be acquired, T_{Total}, can then be summarized as

$$T_{\mathrm{Total}} = \delta_t n_x n_y + T_{\mathrm{LFB}} n_y + T_{\mathrm{FFB}}, \quad (1)$$

where δ_t is the pixel dwell time, n_x and n_y are the number of pixels in x and y, respectively, T_{LFB} is the line flyback time, and T_{FFB} is the frame flyback time (Mullarkey et al., 2022). For example, a relatively fast but typical scan consisting of 512×512 pixels, 1 µs pixel time, and 500 µs line flyback takes over 0.5 s per image, yielding a maximum frame rate of 1.9 frames per second (fps).

Limited scan speeds cause a number of problems. At first, nonrigid distortions from environmental distortions or specimen drift contort crystallography in an image reduces both resolution and strain mapping fidelity. Conveniently, the conventional rectangular scanning used in STEM allows for practical diagnosis and removal of nonrigid distortions from sequentially acquired images (Berkels et al., 2014; Sang & LeBeau, 2014; Jones et al., 2015; Yankovich et al., 2016). Another effect of the slow scan speed is the associated beam damage due to the highly concentrated electron beam (Egerton, 2019). Typical strategies to circumvent this are to acquire multiple images at a faster rate, with the same total-dose incident on the specimen, but with the dose rate significantly reduced (Jones et al., 2017). However, with faster scanning, the signal to noise of individual images is reduced and the reduction in dwell time is limited by the scan and detection hardware (Mittelberger et al., 2018; Ishikawa et al., 2020; Mullarkey et al., 2021). Similarly, the beam current can simply be reduced, though again giving an adverse effect on signal to noise of individual images (Buban et al., 2009). While image series can be reconstructed and averaged to gain signal, this does not help capture dynamic events in the microscope, for example, in *in situ* experiments, where the poor frame rate necessarily limits the temporal sensitivity of experiments.

Received: October 7, 2022. **Revised:** March 27, 2023. **Accepted:** April 24, 2023

Table 1. Overview of Scanning Acquisition Strategies With Corresponding Acquisition Efficiency and Achievable Frames per Second.

Acquisition Strategy	Motivation	Max. Acquisition Efficiency (%)	Max. Achievable fps
Conventional line-sync (50 Hz) and flyback (500 µs) at 512 × 512 px	Ease of use, line-sync mitigates A.C. mains image distortions	97.49	0.098
Reduced dwell time (1 µs) followed by nonrigid registration (Jones et al., 2017)	Faster scanning reduces frame time and effects of environmental distortion	50.59	1.93
Reduced dwell time and reduced flyback time (20 µs) (Mullarkey et al., 2022)	Reduced flyback waiting improves beam efficiency	96.24	3.67
Interlacing (this work)	Reduced number of pixels further reduces frame time	192.48	7.34
Reduced pixel dimensions (256 × 256 px) (Yankovich et al., 2015)		92.75	14.15
Interlacing and reduce image dimensions		185.51	28.31

The acquisition efficiency is defined as the fields of view captured per frame-time dose exposure, with frame time accounting for beam exposure not contributing to data acquisition (e.g., line flyback time).

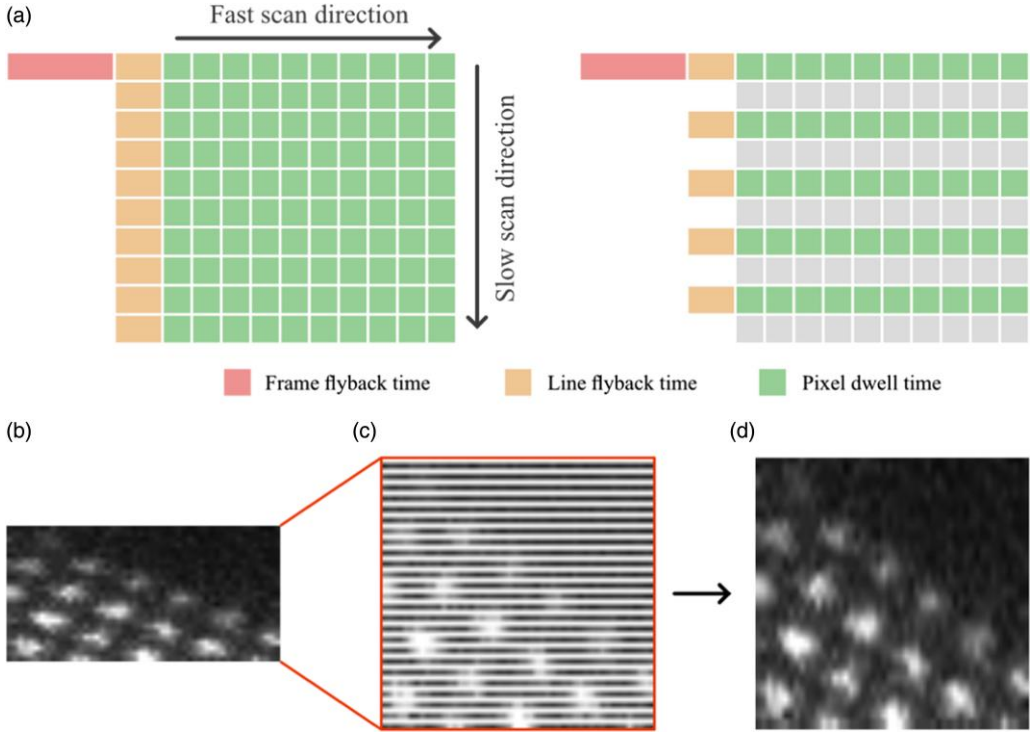

Fig. 1. (**a**) Schematic of full frame and interlaced acquisitions showing the breakdown of total frame time. (**b**) Raw experimental interlaced ADF image of Au columns. (**c**) shows (**b**) with the scan lines spaced correctly in real space and (**d**) shows the image after deinterlacing using bilinear interpolation.

Recent work has shown that the line flyback time can be significantly reduced, without detriment to the retrievable image quality, from typical values of 500 µs to as low as 20 µs (Mullarkey et al., 2022). The remaining option to increase imaging frame rates further is to reduce the number of pixels in an image (Yankovich et al., 2015). Typically, this simply results in a reduced resolution or smaller field of view. A summary of current approaches to STEM acquisition and the corresponding efficiency (i.e., the percentage of acquisition time that produces image data) and fps is given in Table 1. Around 10 years ago, the field of compressed sensing (CS) emerged as an approach to reduce beam damage and decrease frame times. CS uses novel scan paths or high-speed beam blanking to only acquire a subset of pixels in an image, later reconstructing the remainder using computer algorithms (Stevens et al., 2014). There is some doubt as to the advantages of this method (especially when low-dose data become Poisson limited; Van den Broek et al., 2019; Sanders & Dwyer, 2020), though one definite limitation is the requirement for an advanced scan generator or beam blanker (Béché et al., 2016; Li et al., 2018). Uncertainty also surrounds the ability to use CS for quantitative position analysis as nonlinear scan paths introduce hysteresis errors in positioning the beam. The intrinsically sparse nature of CS data also means scan-distortion errors are not readily diagnosed for use with nonrigid registration.

For inspiration to improve scan speeds in current STEM systems, we turn to the early 20th century (Kell et al., 1936). Interlaced video became a widespread technology where only half the lines in a video frame are displayed at once (Fig. 1). Usually frames alternate between showing even and odd lines where, either by human perception or by

computational means, the missing lines can be reconstructed to recover a full frame from each interlaced frame as shown in Figure 1b. The most important aspect of this was, that for the same frame rate and resolution, interlaced video required only half the bandwidth, or storage capacity, as compared with a fully sampled video. Alternatively, for any given transmission bandwidth or storage capacity a doubling of frame rate can be achieved. This has not gone unnoticed in the electron microscopy community, with interlaced scanning used in scanning electron microscopy to limit charging effects (Postek, 2001). However, the differences in resolution and implementation can make this tricky to simply transfer to high-resolution STEM imaging. Most notably, images should be acquired close to Nyquist frequency for an efficient use of beam dose, interlacing may result in acquiring images below Nyquist frequency and reconstructing the missing lines from interlacing (i.e., deinterlacing) may not be straightforward. In STEM, it is also not often possible to alternate between capturing even and odd lines, meaning that video deinterlacing algorithms are not always applicable. On the other hand, interlacing affords us the opportunity to reduce the electron dose by at least a factor of two and, unlike CS, the use of linear scan paths minimizes hysteresis effects in beam positioning and is compatible with existing scan generators and nonrigid registration methods.

Here, we present the application of interlaced scanning and digital super-resolution methods to atomic resolution STEM imaging. We quantitatively evaluate and compare multiple deinterlacing algorithms in the context of single-frame images, image-stack averaging, and image video series. With these results, we present a robust and practical strategy that is applicable to many STEM instruments in use today.

Materials and Methods

Experimental Interlacing

Interlacing is often not readily available on most STEM systems and controllers. If the STEM scan controller has functionality for a custom scan, for example, the point electronic DISS interface, the interlaced scan can be directly programmed (including scan rotation). However, scan controllers that do not directly support such functionality can be made to perform an interlaced scan with relative ease, an advantage of interlaced scans versus other more complicated advanced scans. The majority of scan controllers, for example, Gatan's Digiscan II, have some functionality to control the scan gains (amplifications), usually used to finely tune the scan magnification in x and y. By halving the gain of the noninterlaced scan direction and doubling the number of pixels in the same direction, an interlaced scan can be formed. This approach is trivial to implement but does have some limitations in not being able to realize scan rotation through the scan controller, as is useful for nonrigid registration approaches (Sang & LeBeau, 2014). It is also somewhat nonideal to need to change advanced technical settings between users in a multiuser facility, and could lead to miscalibration of the magnification if set incorrectly.

Deinterlacing

One of the advantages of modern software and programming languages, such as python, is the abundance of publicly available code and libraries for a range of image processing, for example, OpenCV (Bradski, 2000), SciPy (Virtanen et al., 2020), and DIPlib (Luengo et al., n.d.). The range of potential deinterlacing algorithms span a range of complexities, from simple line double to interpolation and advanced in-painting algorithms. Each method has a unique set of advantages and disadvantages, where some may be more robust to noise and others may provide a better reconstruction of images samples close to Nyquist frequency. The implementation of each method used here has been made available in a GitHub for the reader to use or adapt.

Strain Precision

Interlacing provides an interesting opportunity for nonrigid registration to achieve higher strain precisions for a given electron dose. Jones et al. (2017) demonstrated that, for a fixed total dose, the strain precision is proportional to $\frac{1}{\sqrt{n}}$, where n is the number of frames. In theory, interlacing doubles the number of frames for a given dose and should outperform an equivalent dose of full-frame imaging by a factor of $\frac{1}{\sqrt{2}}$. To test this hypothesis, we have developed an approach to incorporate realistic environmental image distortions into simulated image. This allows us to apply the same *time-dependent* distortions (a more realistic approach than pixel dependent) to a series of full frame or interlaced images. To approximate the distortion field, a number of sine waves (typically 50–100) are chosen with random amplitudes, frequencies, phases, and directions. These are then summed and applied to an image in the *time domain* (e.g., accounting for pixel dwell time, flyback wait time, and frame number in the series) using spline interpolation to resample the image. Strains can then be measured using the geometric-phase analysis method (Hÿtch et al., 1998) within the Strain++ software (Peters, 2021). An example of a perfect image of $SrTiO_3$ and its synthetically distorted version are shown in Figure 2a, with the corresponding error in strain demonstrated in Figure 2b. Both the full frame and interlaced simulated and distorted image series can then be nonrigidly aligned and the strain precision measured and fairly compared. It should be noted that there is also potential for interlacing to help with images limited by a low signal-to-noise ratio from low dose and Gaussian noise. Instead of doubling the number of frames, the dwell time of each pixel could be doubled to provide an improvement in signal to noise for fixed total frame time and beam dose.

Results and Discussion

Deinterlacing Comparison

A deinterlacing method suitable for STEM data must first be chosen. To test the various deinterlacing algorithms, we first take a full-frame image and synthetically interlace it, deinterlace it, and compare the result to the original full frame ground truth. The difference between the deinterlaced image and the ground truth reveals any limitations of the deinterlacing approach, as shown in Figure 3a. At the same time, we can measure the algorithm's speed with the goal of determining if real-time deinterlacing is possible under typical experimental conditions.

We tested and compared a range of widely available algorithms, with a subset of popular algorithms shown in Figure 3b. Here the deinterlacing error is defined as the root mean square error from the ground truth. The algorithms examined include: (1) Line doubling, where each line is simply repeated twice; (2) Bilinear interpolation, assuming

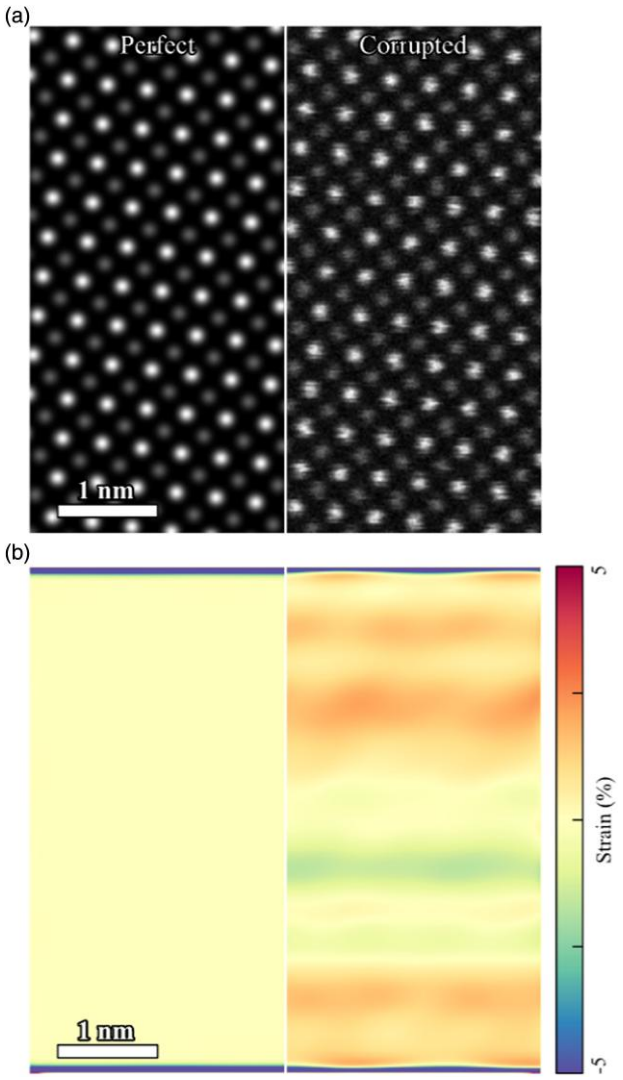

Fig. 2. (**a**) Example simulated image shown before and after distortions have been introduced (scan-corrupted). (**b**) e_{yy} Strain measurement from the perfect and corrupted image shown in (**a**). A full distortion analysis is shown in the Supplementary Material.

interpolated points lie on a linear gradient between adjacent points; (3) Custom bilinear interpolation, where information is incorporated from the fast scan direction; (4) Lanczos interpolation, a resampling method that can preserve sharp edges (Duchon, 1979); (5) Bicubic interpolation, using polynomials to interpolate data between nearest points; (6) FFT boxcar resampling, removing frequencies in the Fourier transform above the interlacing frequency; (7) Telea inpainting provided by OpenCV (Telea, 2004); and (8) Navier Stokes inpainting provided by OpenCV (Bertalmío et al., 2001). The output of a more extensive set of algorithms is shown and compared in Supplementary Figure S3. The code to reproduce Figure 3 has been made available on GitHub (https://github.com/TCD-Ultramicroscopy/STEM-deinterlacing), so that the reader can examine the deinterlacing algorithms as well as test with their own algorithms, their own images, or their own hardware.

While the exact results of Figure 3 can vary between images, and we encourage the reader to test the algorithms for their specific imaging conditions and needs, some preferred approaches start to emerge. For example, line doubling stands out as the fastest method, with bicubic interpolation giving the best error from the ground truth. There are then compromises such as bilinear interpolation, with speeds closer to line doubling, but with an error closer to bicubic. Because of this, and the ease of implementation in different programming languages, bilinear interpolation has been chosen as the default deinterlacing method for the work presented here. Perhaps disappointingly, the advanced inpainting algorithms give some of the highest error for the lowest speeds, though it should be noted that the computation speed is somewhat subjective as it depends on the required scanning speed as well as the specific hardware. Equally the speed depends on the specific algorithm, for example, the two bicubic interpolation implementations from the DIPLib (Luengo et al., n.d.) and SciPy (Virtanen et al., 2020) libraries have drastically different speeds. Further to this, large improvements in speed might be realized using multithreading or graphical processing units.

Frame rates

The maximum possible frame-rate improvement from interlacing is a factor of two. However, frame flyback can limit the achievable frame rate, potentially consisting of data streaming from the scan controller to the computer, copying/saving data, and factors internal to the scan generator. To compare the experimental frame-rate improvements from interlacing, a summary of frame times is given in Table 2. We have tested an FEI Titan G2, equipped with a point electronic DISS scan control, as well as a Nion UltraSTEM 200 and JEOL ARM200F, both equipped with a Gatan Digiscan II. The frame rates from the Digiscan II only show a speed improvement of 64% when interlacing. This is due to an extra interframe time from equation (1) measured to be 0.154 ± 0.005 s, independent of scan size, that limits the achievable frame rate. The point electronic DISS controller significantly reduced the interframe time, allowing interlacing to achieve a 99.5% increase in frame rate compared with full-frame imaging. In any case, interlacing gives a significant improvement in imaging frame rate for minimal penalty.

Strain Precision

To compare the strain precision of images with varying dose fractionation but equal total dose, an artificial, strain-free image of [100] $SrTiO_3$ was generated as a series of Gaussians at 512×512 pixel size (a detailed multislice simulation is not necessary for this analysis). Pixel dwell times, δ_t, and total number of frames, n, were chosen for full frames and interlaced frames such that $\delta_t \cdot n$ was 40 and 80 µs, respectively. For a fixed dose, interlacing gives the freedom to double either the number of frames or the dwell time. For images with Gaussian noise and low electron doses, doubling the dwell time may be desired to achieve a sufficient signal-to-noise ratio. Alternatively, the number of frames can be doubled with the aim of reducing the strain error, as is the approach taken here. Distortions representing the effects of environmental disturbances were then generated (with behaviors matched fairly with respect to time rather than scan location) and applied to both the full frame and the interlaced series with and without 90° scan rotation between frames. Interlaced images were then deinterlaced using bilinear interpolation, and each image series was then nonrigidly aligned with SmartAlign (Jones et al., 2015), using the same settings throughout. The strain

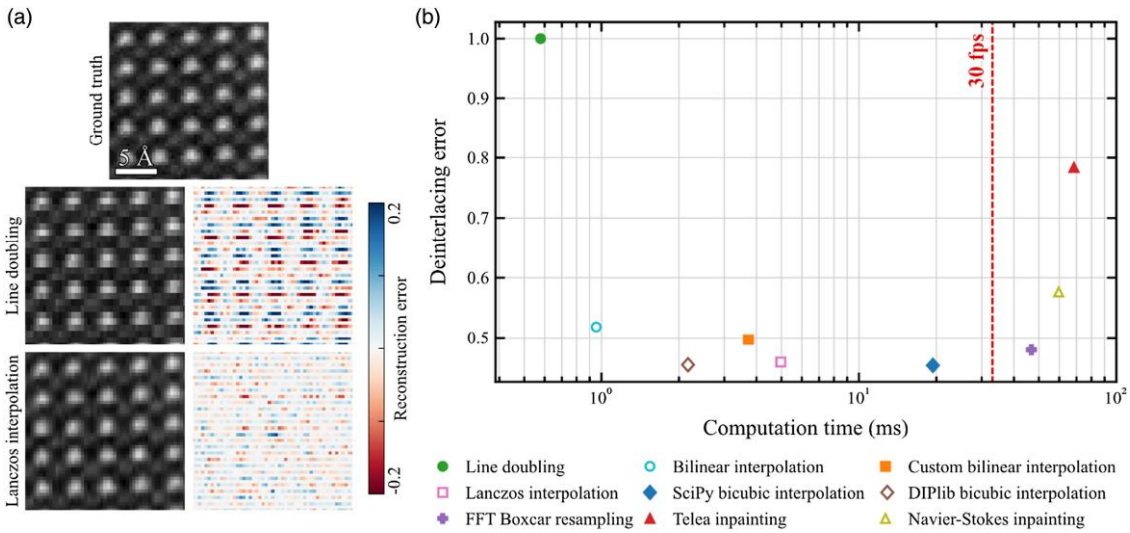

Fig. 3. (**a**) Ground truth experimental ADF image of $PbZr_{0.2}Ti_{0.8}O_3$ with exemplar line-doubled and Lanczos deinterlaced images. The difference to the ground truth is shown as a fraction of the intensity range of the ground truth image. (**b**) Deinterlacing error versus computation time. Deinterlacing error is calculated as the root mean square error. Times are an average of 1,000 calculations performed on an Intel i7-10700. The ground truth image in (**a**) is a crop of the image used to calculate the deinterlacing error in (**b**). The full image and expanded plot of (**b**) can be found in the Supplementary Material.

Table 2. Expected and Experimentally Achieved Frame Rates for Conventional and Interlaced Imaging With a Given set of Scan Parameters.

Pixel Dwell Time (µs)	Line Flyback Time (µs)	Scan Width (Pixels)	Scan Height (pixels)	Scan Controller	Expected fps	Achieved fps
3	500	300	300	Gatan Digiscan II	2.38	1.74 ± 0.02
			150		4.76	2.85 ± 0.03
			300	Point electronic DISS	2.38	2.3701 ± 0.0006
			150	6	4.76	4.728 ± 0.004

error, which on a perfect single crystal is any deviation from 0% strain, was then quantified as the standard deviation of the ε_{yy} strain component (Hÿtch et al., 1998), where the ε_{yy} component was chosen as most of the strain error is expected in the slow y-scan direction compared with the fast x-scan direction, assuming no scan rotation.

If we consider that the apparent probe displacements resulting from randomized uncorrelated scan distortions have a Gaussian-like distribution (Jones et al., 2017), then following frame averaging the width of the distribution describing these would be expected to reduce with a $\frac{1}{\sqrt{n}}$ relationship (where n is the number of frames averaged). The resulting strain error of the full frame and interlaced series is shown in Figure 4a for simulated data as a function of the number of dose equivalent full frames (i.e., the number of experimentally recorded probe positions divided by the number of image pixels). The $\frac{1}{\sqrt{n}}$ proportionality is immediately visible from the fit lines in all cases.

The imaging strategy with the largest strain error is the full-frame imaging with no scan rotation between frames, as would be expected from the literature. The equivalent interlaced strain precision is a factor of 1.59 ± 0.07 lower (better), exceeding the expected $\sqrt{2}$ (1.41) improvement. This better-than-expected improvement may be a result of halving the apparent strain gradient in the deinterlaced image due to the two times faster sampling of the distortion field in the interlaced approach. The reduced apparent strain gradient is likely better diagnosed and corrected by the nonrigid registration in SmartAlign. Interestingly, the full-frame images with scan rotation also give a similar 1.61 ± 0.09 improvement compared with full-frame imaging, perhaps because of the orthogonal redundant views of the same sample. A further 1.26 ± 0.03 improvement in the strain precision is found by combining scan rotation with the interlaced acquisition, giving a total improvement of 2.0 ± 0.1 from the full-frame series without rotation. The strain precision improvement from interlaced to interlaced with rotation of 1.264 ± 0.005 suggest that, while still a significant improvement, interlacing benefits less from scan rotation. This is possibly because the ε_{yy} strain component is already improved from partially measuring the fast scan direction and interlacing only provides an improvement to the frames where the slow scan direction is collinear with the measured strain orientation. In any case, the maximum strain precision for a given dose budget is achieved when using STEM interlacing with scan rotation between frames.

As the simulated measurements of Figure 4a are under synthetic conditions with purely Poisson noise behavior, these findings were verified experimentally. Figure 4b shows the equivalent measurement of strain precision from a JEOL ARM200F (double corrected, operating at 200 kV with a convergence semiangle of 23 mrad) controlled by a Digiscan II, with full-frame images captured at a resolution of 512×512 and flyback time set at 500 µs. As mentioned earlier, the Gatan Digiscan II hardware configuration does not support automated acquisition of interlaced images

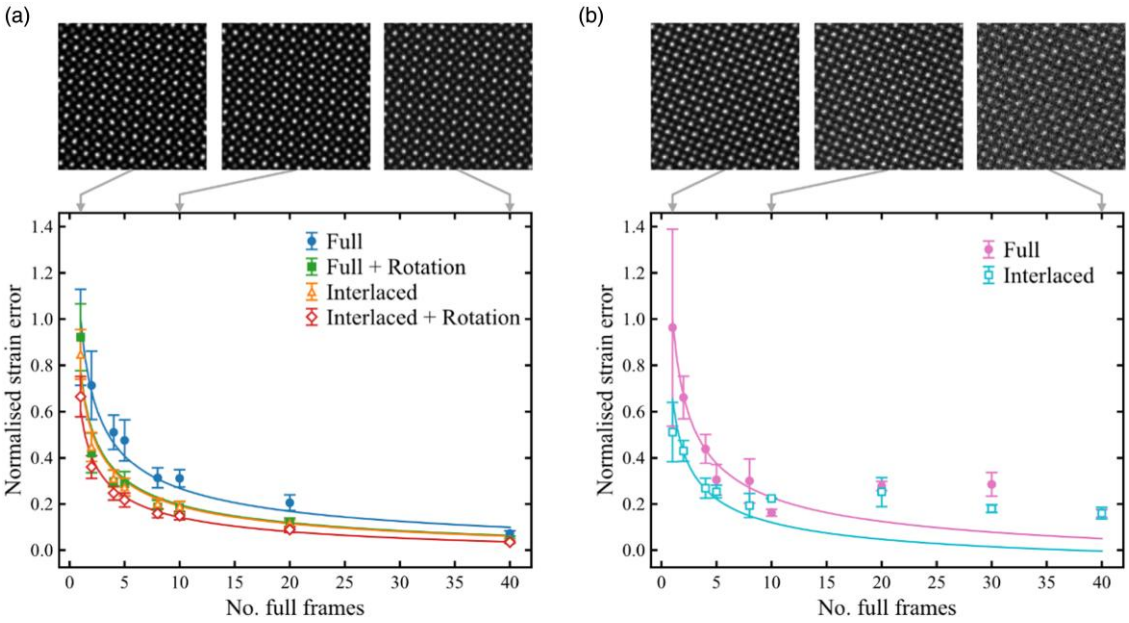

Fig. 4. Strain error of reconstructed images as a function of dose fractionation and across different scanning strategies. (**a**) and (**b**) show simulated and experimental data, respectively, with example single frames show above. Fit lines are $\propto \frac{1}{\sqrt{n}}$ and error bars show the standard error of the means. Strain error has been normalized to the full-frame data fit lines at $n = 1$.

with scan rotation. Similar to previous works by Jones et al. (2017), at higher dose fractionation (the noisiest images), the strain precision does not continue to decrease endlessly with the expected $\frac{1}{\sqrt{n}}$ proportionality. A discussion of this effect has been presented in the Supplementary Material, with a probable cause being higher frequency environmental distortions. In this case, further improvements to strain precision necessitate improved microscope or room/environment designs (Muller et al., 2006). Despite this limitation, an improvement in strain precision is still achieved, with a factor of 1.4 ± 0.1 improvement again agreeing with the expected value of $\sqrt{2}$. With our experimental measurements, it can be seen that a dose fractionation using interlacing of 20 frames (equivalent to 10 full frames) provides the best strain precision for a fixed dose. The reader is encouraged to reproduce this optimization for their own conditions (e.g., sample material or detector angles) but this serves as a reasonable starting condition.

Conclusion

We have demonstrated the applicability and utility of interlacing to atomic resolution STEM imaging using simple, readily available, and computationally efficient algorithms. Acquiring interlaced STEM images does not require further financial investment in hardware or software, providing an accessible and sustainable method to increasing the capabilities of any existing STEM. Interlacing provides an easy way to double imaging frame rates, reduce dose rate, and allow dynamic *in situ* events to be captured while remaining compatible with existing nonrigid registration techniques. The methods explored here are easily implemented and can also provide benefits to spectroscopic or 4D imaging. In particular, interlaced STEM combined with scan rotation and nonrigid registration achieved the highest strain precision for a fixed total dose budget compared with conventional full-frame imaging.

Availability of Data and Materials

The code which is used to test deinterlacing methods, add distortions to images, and measure strain can be found at our Github repository https://github.com/TCD-Ultramicroscopy/STEM-deinterlacing. The data used in this paper can be found at doi: 10.5281/zenodo.7137495.

Supplementary Material

To view supplementary material for this article, please visit https://doi.org/10.1093/micmic/ozad056.

Acknowledgments

The authors acknowledge the Centre for Research on Adaptive Nanostructures and Nanodevices (CRANN) and the Advanced Materials and BioEngineering Research (AMBER) Network for support for this work. In particular, we acknowledge the help and support of the Advanced Microscopy Laboratory (AML) staff and facilities. E.N. as an undergraduate at the time acknowledges the support of the Trinity College Dublin School of Physics.

Financial Support

J.J.P.P. and L.J. acknowledge SFI grant 19/FFP/6813, L.J. acknowledges SFI/Royal Society Fellowship grant URF/RI/191637, T.M. acknowledges the SFI & EPSRC Centre for Doctoral Training in the Advanced Characterisation of Materials (award references 18/EPSRC-CDT-3581 and EP/S023259/1). J.A.G. acknowledges EPSRC grant EP/P031544/1.

Conflict of Interest

The authors declare that they have no competing interest.

References

Béché A, Goris B, Freitag B & Verbeeck J (2016). Development of a fast electromagnetic beam blanker for compressed sensing in scanning transmission electron microscopy. *Appl Phys Lett* **108**, 093103. https://doi.org/10.1063/1.4943086

Berkels B, Binev P, Blom DA, Dahmen W, Sharpley RC & Vogt T (2014). Optimized imaging using non-rigid registration. *Ultramicroscopy* **138**, 46–56. https://doi.org/10.1016/j.ultramic.2013.11.007

Bertalmío M, Bertozzi AL & Sapiro G (2001). Navier-Stokes, fluid dynamics, and image and video inpainting. In Proceedings of the 2001 IEEE Computer Society Conference on Computer Vision and Pattern Recognition. CVPR 2001 1, I-355-I–362.

Bradski G (2000). The OpenCV library. *Dr. Dobb's J Softw Tools* **120**, 122–125.

Buban JP, Ramasse Q, Gipson B, Browning ND & Stahlberg H (2009). High-resolution low-dose scanning transmission electron microscopy. *J Electron Microsc (Tokyo)* **59**, 103–112. https://doi.org/10.1093/jmicro/dfp052

Duchon CE (1979). Lanczos filtering in one and two dimensions. *J Appl Meteorol* **18**, 1016–1022. https://doi.org/10.1175/1520-0450(1979)018<1016:LFIOAT>2.0.CO;2

Egerton RF (2019). Radiation damage to organic and inorganic specimens in the TEM. *Micron* **119**, 72–87. https://doi.org/10.1016/j.micron.2019.01.005

Hÿtch MJ, Snoeck E & Kilaas R (1998). Quantitative measurement of displacement and strain fields from HREM micrographs. *Ultramicroscopy* **74**, 131–146. https://doi.org/10.1016/S0304-3991(98)00035-7

Ishikawa R, Jimbo Y, Terao M, Nishikawa M, Ueno Y, Morishita S, Mukai M, Shibata N & Ikuhara Y (2020). High spatiotemporal-resolution imaging in the scanning transmission electron microscope. *Microscopy* **69**, 240–247. https://doi.org/10.1093/jmicro/dfaa017

Jones L, Wenner S, Nord M, Ninive PH, Løvvik OM, Holmestad R & Nellist PD (2017). Optimising multi-frame ADF-STEM for high-precision atomic-resolution strain mapping. *Ultramicroscopy* **179**, 57–62. https://doi.org/10.1016/j.ultramic.2017.04.007

Jones L, Yang H, Pennycook TJ, Marshall MSJ, Aert SV, Browning ND, Castell MR & Nellist PD (2015). Smart align—A new tool for robust non-rigid registration of scanning microscope data. *Adv Struct Chem Imaging* **1**, 1–6. https://doi.org/10.1186/s40679-015-0008-4

Kell RD, Bedford AV & Trainer MA (1936). Scanning sequence and repetition rate of television images. *Proc Inst Radio Engineers* **24**, 559–576.

Li X, Dyck O, Kalinin SV & Jesse S (2018). Compressed sensing of scanning transmission electron microscopy (STEM) with nonrectangular scans. *Microsc Microanal* **24**, 623–633. https://doi.org/10.1017/S143192761801543X

Luengo C, *et al.* (n.d.). DIPlib: Quantitative image analysis in C++, MATLAB and Python. Available at https://github.com/DIPlib/diplib. Accessed March 2023.

Mittelberger A, Kramberger C & Meyer JC (2018). Software electron counting for low-dose scanning transmission electron microscopy. *Ultramicroscopy* **188**, 1–7. https://doi.org/10.1016/j.ultramic.2018.02.005

Mullarkey T, Downing C & Jones L (2021). Development of a practicable digital pulse read-out for dark-field STEM. *Microsc Microanal* **27**, 99–108. https://doi.org/10.1017/S1431927620024721

Mullarkey T, Peters JJP, Downing C & Jones L (2022). Using your beam efficiently: Reducing electron dose in the STEM via flyback compensation. *Microsc Microanal* **28**, 1428–1436. https://doi.org/10.1017/S1431927621013908

Muller DA (2009). Structure and bonding at the atomic scale by scanning transmission electron microscopy. *Nat Mater* **8**, 263–270. https://doi.org/10.1038/nmat2380

Muller DA, Kirkland EJ, Thomas MG, Grazul JL, Fitting L & Weyland M (2006). Room design for high-performance electron microscopy. *Ultramicroscopy* **106**, 1033–1040. https://doi.org/10.1016/j.ultramic.2006.04.017

Ophus C (2019). Four-dimensional scanning transmission electron microscopy (4D-STEM): From scanning nanodiffraction to ptychography and beyond. *Microsc Microanal* **25**, 563–582. https://doi.org/10.1017/S1431927619000497

Peters JJP (2021). Strain++ v1.7. https://zenodo.org/record/5020766.

Postek MT (1984). Critical dimension measurement in the scanning electron microscope. *Proc. SPIE 0480, Integrated Circuit Metrology II*, 109–119. doi: https://doi.org/10.1117/12.943055

Sanders T & Dwyer C (2020). Inpainting versus denoising for dose reduction in scanning-beam microscopies. *IEEE Trans Image Process* **29**, 351–359. https://doi.org/10.1109/TIP.2019.2928133

Sang X & LeBeau JM (2014). Revolving scanning transmission electron microscopy: Correcting sample drift distortion without prior knowledge. *Ultramicroscopy* **138**, 28–35. https://doi.org/10.1016/j.ultramic.2013.12.004

Sasaki T, Sawada H, Okunishi E, Hosokawa F, Kaneyama T, Kondo Y, Kimoto K & Suenaga K (2012). Evaluation of probe size in STEM imaging at 30 and 60 kV. *Micron* **43**, 551–556. https://doi.org/10.1016/j.micron.2011.10.010

Stevens A, Yang H, Carin L, Arslan I & Browning ND (2014). The potential for Bayesian compressive sensing to significantly reduce electron dose in high-resolution STEM images. *Microscopy* **63**, 41–51. https://doi.org/10.1093/jmicro/dft042

Telea A (2004). An image inpainting technique based on the fast marching method. *J Graph Tools* **9**, 23–34. https://doi.org/10.1080/10867651.2004.10487596

Van den Broek W, Reed BW, Béché BW, Verbeeck A, & Koch J & T C (2019). Viability of compressed sensing as a dose reduction strategy in STEM. *Microsc Microanal* **25**, 1686–1687. https://doi.org/10.1017/S1431927619009164

Virtanen P, Gommers R, Oliphant TE, Haberland M, Reddy T, Cournapeau D, Burovski E, Peterson P, Weckesser W & Bright J (2020). Scipy 1.0: Fundamental algorithms for scientific computing in Python. *Nat Methods* **17**, 261–272. https://doi.org/10.1038/s41592-019-0686-2

Yankovich AB, Berkels B, Dahmen W, Binev P & Voyles PM (2015). High-precision scanning transmission electron microscopy at coarse pixel sampling for reduced electron dose. *Adv Struct Chem Imaging* **1**, 2. https://doi.org/10.1186/s40679-015-0003-9

Yankovich AB, Zhang C, Oh A, Slater TJA, Azougb F, Freer R, Haigh SJ, Willett R & Voyles PM (2016). Non-rigid registration and non-local principle component analysis to improve electron microscopy spectrum images. *Nanotechnology* **27**, 364001. https://doi.org/10.1088/0957-4484/27/36/364001